Supporting Information

Electrochemical Anilinium Reduction: Identifying Metastable Surface Intermediate on Pt and Its Voltage-Driven Decomposition to Hydrogen Evolution

Dayeon Park†,[a], Cheolmin Park†,[a], SeungJae Kwak†,[b], Dongho Seo†,[c], Dongmin Kim[d], Won bo Lee[b], Ki Min Nam[c],*, YongJoo Kim[d],*, Jinho Chang[a],*

[a]Department of Chemistry and Research Institute for Convergence of Basic Science, Hanyang University, Seoul 04763, Republic of Korea

[b]School of Chemical and Biological Engineering, Institute of Chemical Processes, Seoul National University, Seoul 08826, Republic of Korea

[c]Department of Chemistry and Chemistry institute of Functional Materials, Pusan National University, Busan 46241, Republic of Korea

[d]Department of Materials Science and Engineering, Korea University, Seoul 02841, Republic of Korea

Table of Contents

Figure S1. ………………………………………………………………… S-1

CVs associated with HER in (a) a 10 mM $HClO_4$ and (b) the same concentration of AnH^+ solution measured through EQCM cell. In all the solutions, 0.1 M $NaClO_4$ was added as a supporting electrolyte and the scan rate of all the CVs was 20 mV/s.

Figure S2. ………………………………………………………………… S-2

The representative Δf vs. t curves through the EQCM at various E_{appl} in 10 mM $HClO_4$ solutions: E_{appl} = (a) 0, (b) -0.3, (c) -0.6, (d) -0.8, (e) -1, (f) -1.2, and (g) -1.4 V.

Figure S3. ………………………………………………………………… S-3

Δf vs. t curves obtained from the EQCM cell in 10 mM AnH^+ solutions at E_{appl} = -0.8 V on Pt electrodes, which underwent different pre-treatments. The Pt electrodes were rinsed with either (a) deionized water or (b) a 10 mM AnH^+ solution, after applying a constant potential of -0.8 V in a 10 mM AnH^+ solution.

Figure S4. ………………………………………………………………… S-4

The representative Δf vs. t curves through the EQCM measurements at various E_{appl} in the 10 mM An solutions: (a) 0, (b) -0.3, (c) -0.6, (d) -0.8, (e) -1, (f) -1.2, and (g) -1.4 V.

Figure S5. ………………………………………………………………… S-5

A representative Δf vs. t curve through the EQCM measurement in a solution containing 50 mM AnH^+ at a constant -0.8 V.

Figure S6. ………………………………………………………………… S-6

(a-b) Snapshots of hydrogen bubbles on Pt electrodes at ~180 s during the chronoamperometry in the two different solutions; hydrogen bubbles with smaller sizes were observed in the 0.1 M AnH^+ solution than in the 0.1 M $HClO_4$. (c) CVs of HER at 0.01 V/s measured in (black) 0.1 M $HClO_4$ and (blue) 0.1 M AnH^+, (d) chronoamperograms from each solution at the different E_{appl} to maintain nearly identical current density at quasi steady state.

Figure S7. ………………………………………………………………… S-7

(a) CVs from the in situ GC electrochemical cell in solutions containing either 10 mM H^+ (black line) and the same concentration of AnH^+ (red line) at 20 mV/s, and (b) the resultant FE_{H2} vs. E_{appl} plots. GC spectra of obtained at –1.0 V vs. Ag/AgCl in (c) H^+ and (d) AnH^+ solutions.

Figure S8. ………………………………………………………………… S-8

The simulated concentration profile at the maximum voltammetric current shown in Figure 3a.

Note S1. ………………………………………………………………… S-9

Finite element method for voltammetric simulation for HER induced by H^+ and AnH^+-reduction on an UME.

Figure S9. ·· S-10

Description of the 2D axial domain of the finite element analysis for the voltammetric simulation.

Figure S10. ·· S-11

Representative CVs of HER at 20 mV/s in $HClO_4$ solutions with various $C_{H^+}^{bulk}$: (a) 10, (b) 50, (c) 100, (d) 150, (e) 200, (f) 300, (g) 400, and (h) 500 mM. We note that CVs at $C_{H^+}^{bulk}$ = 50 mM show the intermediate behavior, which gave either the limiting current or sudden current drop.

Figure S11. ·· S-12

A CV at 20 mV/s in a 150 mM AnH^+ solution on a Pt UME and the voltammetric simulation result.

Figure S12. ·· S-13

Representative *i-t* curves with/without the current spike measured from a same aqueous solution with 150 mM AnH^+ at E_{appl} = -0.95 V.

Figure S13. ·· S-14

Representative *i-t* curve which was hard to resolve the t_{spike} of the current spike due to a capacitive current from aqueous solution with 150 mM AnH^+ at E_{appl} = -1.2 V.

Figure S14. ·· S-15

Representative CVs of HER at 20 mV/s in solutions with various concentration of AnH^+ = (a) 150, (b) 200, (c) 250, (d) 300 mM.

Figure S15. ·· S-16

The background CV measured in 0.1 M $NaClO_4$ solution at 20 mV/s without either AnH^+ or An.

Figure S16. ·· S-17

The representative *i-t* curves (a, c) with/(b, d) without a current spike asscociated with $[An\text{-}H]_{ads}$-reduction at E_{appl} = -1.3 V in a 150 mM AnH^+ solution with $C_{An}^{bulk}/C_{AnH^+}^{bulk}$ = 1. (c) and (d) are the magnified *i-t* curves at $t \leq 0.2$ s from those in (a) and (b), respectively.

Figure S17. ·· S-18

Δf vs. t curves with three replicates in solutions containing 50 mM AnH^+ with different C_{An}^{bulk} at E_{appl} = -0.8 V: C_{An}^{bulk} = (a) 0, (b) 25, (c) 50, (d) 100, and (e) 250 mM, respectively.

Figure S18. ·· S-19

Representative Nyquist plots associated with HER of AnH^+ in different $C_{An}^{bulk}/C_{AnH^+}^{bulk}$ = (a) 0, (b) 0.5, (c) 1, (d) 2, and (e) 5 at $C_{AnH^+}^{bulk}$ = 50 mM, and (f) the equivalent circuit model for EIS simulation fitting to the experimental results. In this circuit model, $R_{ct,1}$ and $R_{ct,2}$ are the charge transfer resistance at an interface of Pt and that of $[An\text{-}H]_{ads}$, respectively. R_u is the uncompensated resistance, CPE is the constant phase element, and Z_w is the Warburg impedance.

Figure S19. ………………………………………………………………… S-20

Enlarged figures of the corresponding geometries in the two-AnH adsorption mechanism. Hydrogen bonds are marked by black dashed lines, while height between the aromatic centers and Pt are marked by red arrow dashed lines.

Figure S20. ………………………………………………………………… S-21

Alternative adsorption configurations evaluated using PBE-D3. (a) Adsorption of an An molecule. (b) Alternative adsorption configuration of PtH–An. (c–f) PtH–An–HAn structures optimized from different initial stacking directions, with H adsorbed on a Pt-top site (c–e) and a Pt-hollow site (f). (g, h) PtH–AnH–An structures with H adsorbed on a Pt-top site (g) and a Pt-hollow site (h). The numbers beneath each image indicate relative energies with respect to the most stable configurations shown in Fig. 6a.

Figure S21. ………………………………………………………………… S-22

Top view of the Charge density difference of adsorption of the three representative An(H), displaced in Figure 6c-e.

Figure S22. ………………………………………………………………… S-23

DFT calculated reaction diagrams for different functionals and application of dispersion corrections. (a) PBE, (b) RPBE. (c) RPBE-D3, (d) PBEsol, and (e) PBEsol-D3 at -0.56 V vs. Ag/AgCl.

Figure S23. ………………………………………………………………… S-24

DFT optimized structures for different functionals and dispersion corrections. i-v indicates the reaction states corresponding to that of Figure 6a. Each row corresponds to (a) PBE, (b) RPBE-D3, (c) RPBE, (d) PBEsol-D3, and (e) PBEsol, where i-v correspond to the structures found in Figure 6. Note for e, only four structures are shown, omitting PtH···AnH···An (the iv structure), which after optimization falls back to PtH···An···HAn (iii). The heights between the aromatic centers and Pt are marked by red arrow dashed lines with corresponding distances (Å).

Note S2. ………………………………………………………………… S-25,26

Comparison of different functionals and dispersion corrections.

Table S1. ………………………………………………………………… S-27

The simulation parameters for electrode reaction and chemical reaction in Figure 1c; the standard reduction potential, transfer coefficient, standard electron transfer rate constant, equilibrium constant, forward rate constant, diffusion coefficients and concentrations of species, *i* are designated as E^{o}, α, k^{0}, K_{eq}, k_f, D_i, and C_i, respectively.

Table S2. ………………………………………………………………………… S-28

The simulation parameters for electrode reaction and chemical reaction through CE process in Figure 1c.

Table S3. ………………………………………………………………………… S-29

The simulation parameters for electrode reaction and chemical reaction through combined CE + EC process in Figure 1c.

Table S4. ………………………………………………………………………… S-30

The simulation parameters for electrode reaction and chemical reaction in Figure 3.

Table S5. ………………………………………………………………………… S-31

The simulation parameters for electrode reaction and chemical reaction in Figure S11.

Table S6. ……………………………………………………………………… S-32,33

Optimized structural parameters for the various An and AnH configurations in different functionals, represented in Figure 6a and Figure S23.

References. ……………………………………………………………………… S-34

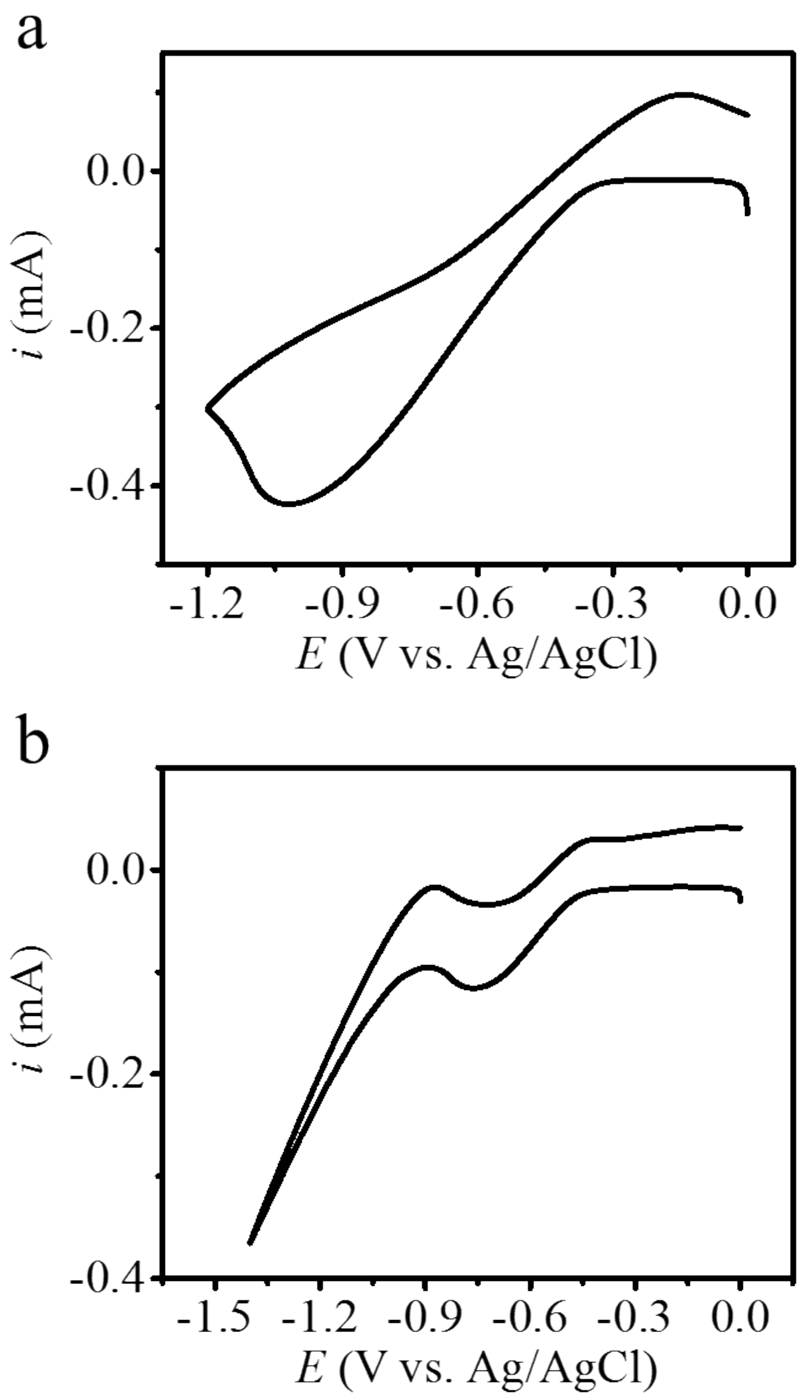

Figure S1. CVs associated with HER in (a) a 10 mM $HClO_4$ and (b) the same concentration of AnH^+ solution measured through EQCM cell. In all the solutions, 0.1 M $NaClO_4$ was added as a supporting electrolyte and the scan rate of all the CVs was 20 mV/s.

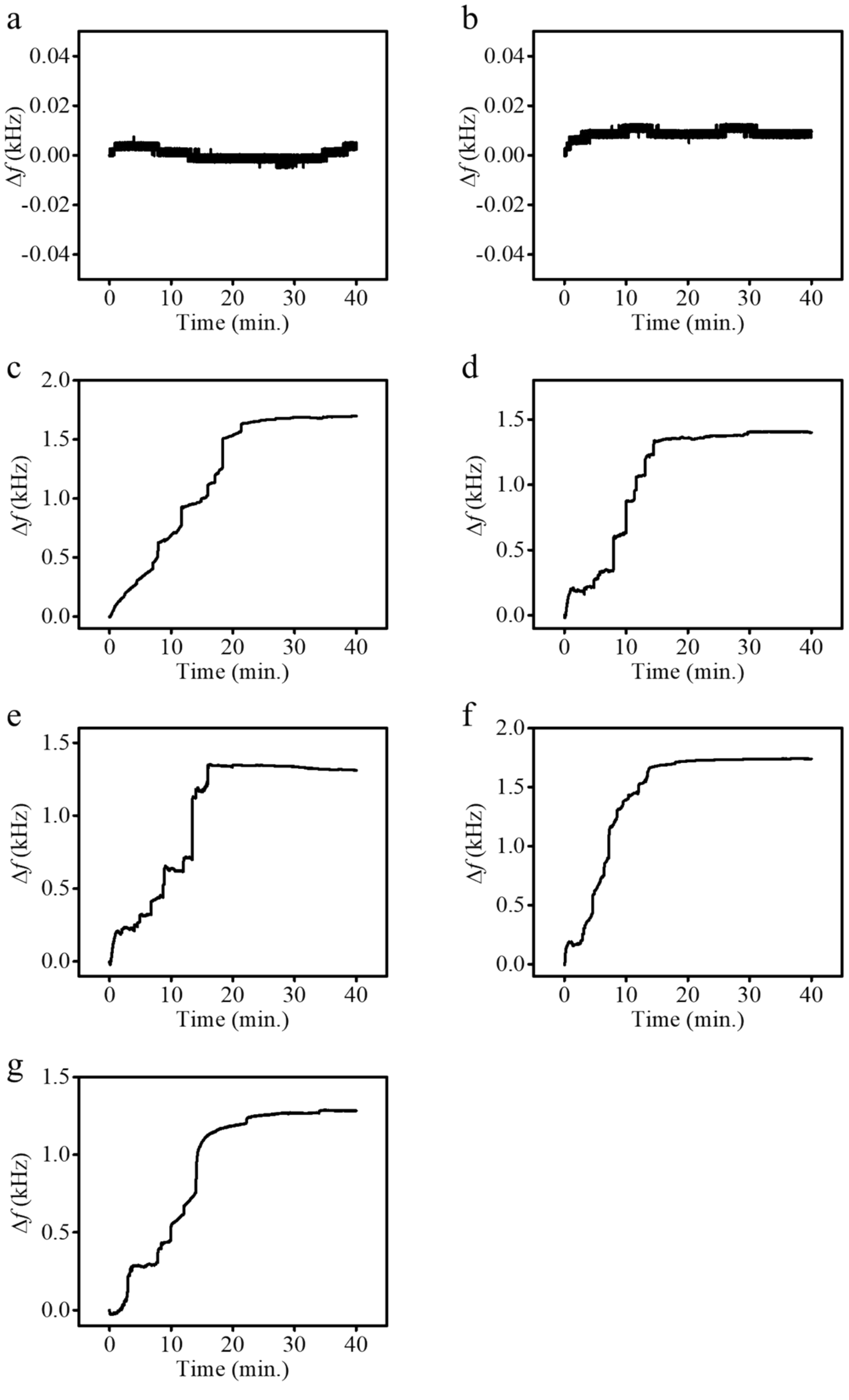

Figure S2. The representative Δ*f* vs. *t* curves through the EQCM at various E_{appl} in 10 mM $HClO_4$ solutions: E_{appl} = (a) 0, (b) -0.3, (c) -0.6, (d) -0.8, (e) -1, (f) -1.2, and (g) -1.4 V.

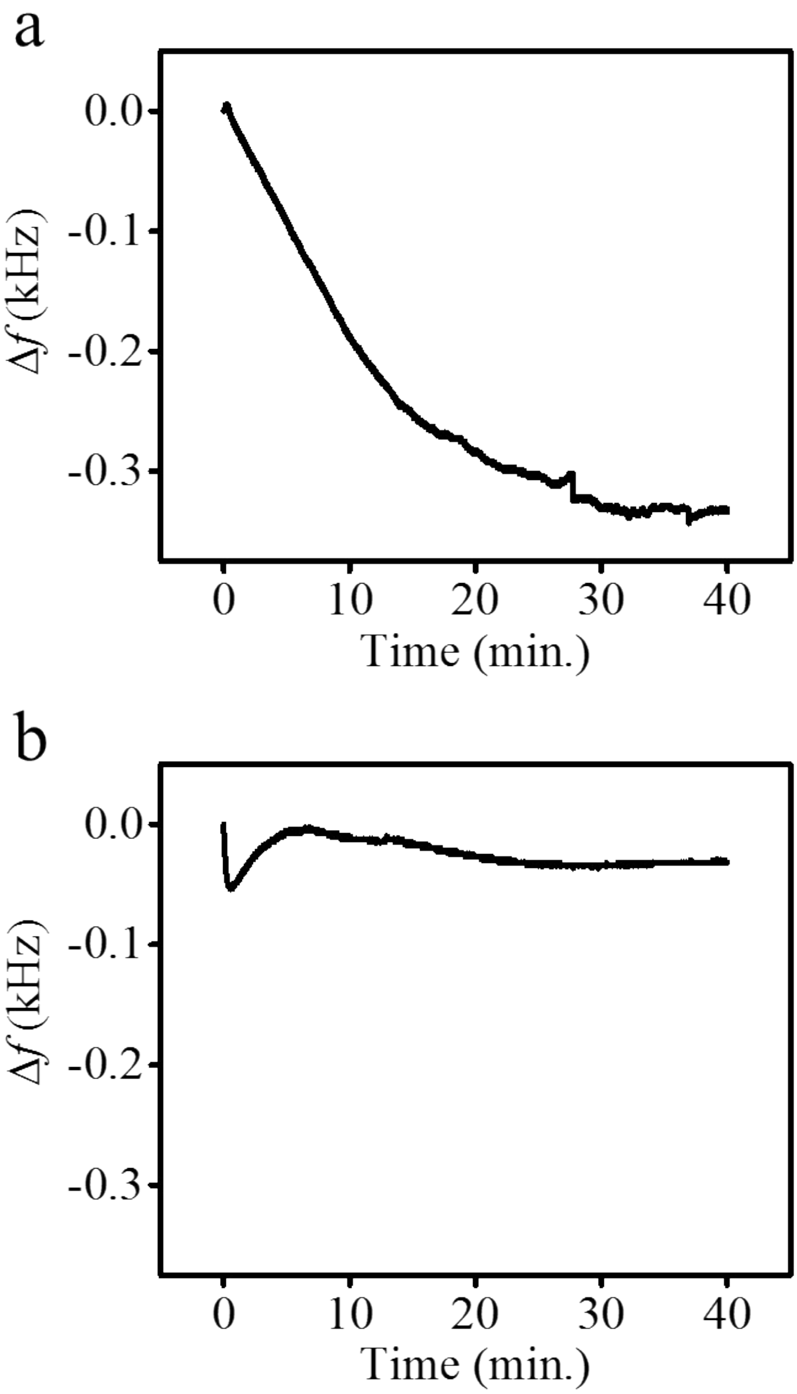

Figure S3. Δf vs. t curves obtained from the EQCM cell in 10 mM AnH^+ solutions at E_{appl} = -0.8 V on Pt electrodes, which underwent different pre-treatments. The Pt electrodes were rinsed with either (a) deionized water or (b) a 10 mM AnH^+ solution, after applying a constant potential of -0.8 V in a 10 mM AnH^+ solution.

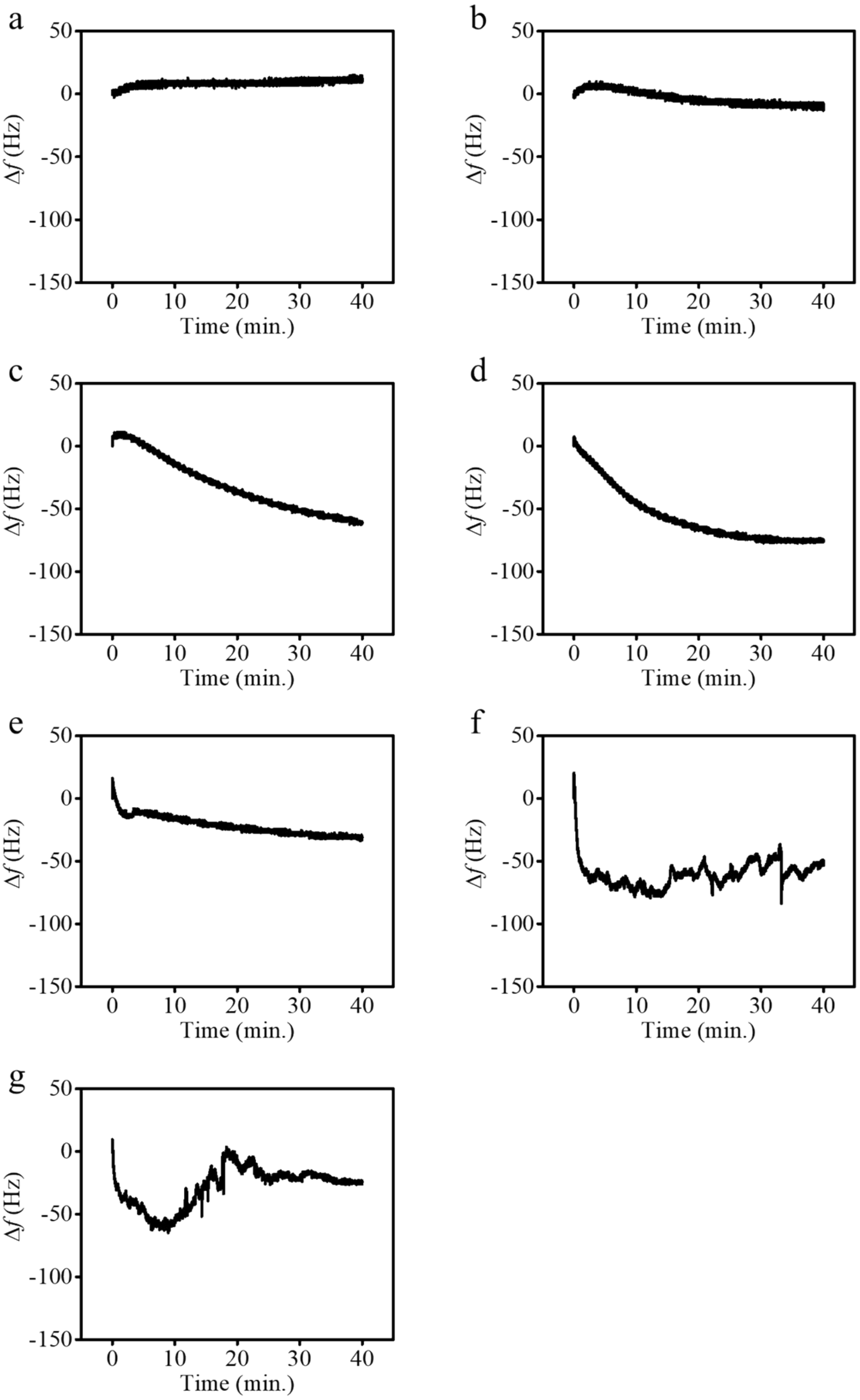

Figure S4. The representative Δ*f* vs. *t* curves through the EQCM measurements at various E_{appl} in the 10 mM An solutions: (a) 0, (b) -0.3, (c) -0.6, (d) -0.8, (e) -1, (f) -1.2, and (g) -1.4 V.

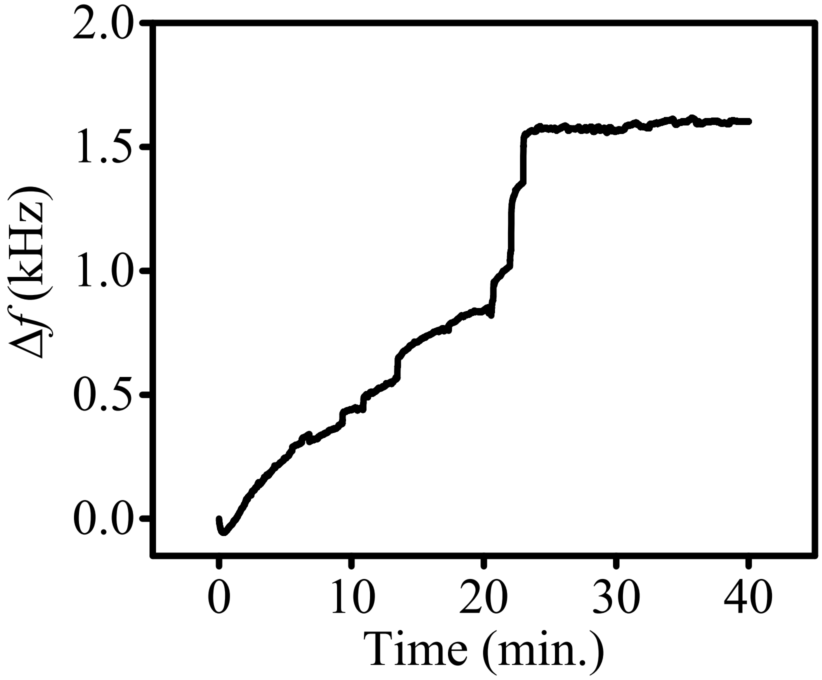

Figure S5. A representative Δ*f* vs. *t* curve through the EQCM measurement in a solution containing 50 mM AnH^+ at a constant -0.8 V.

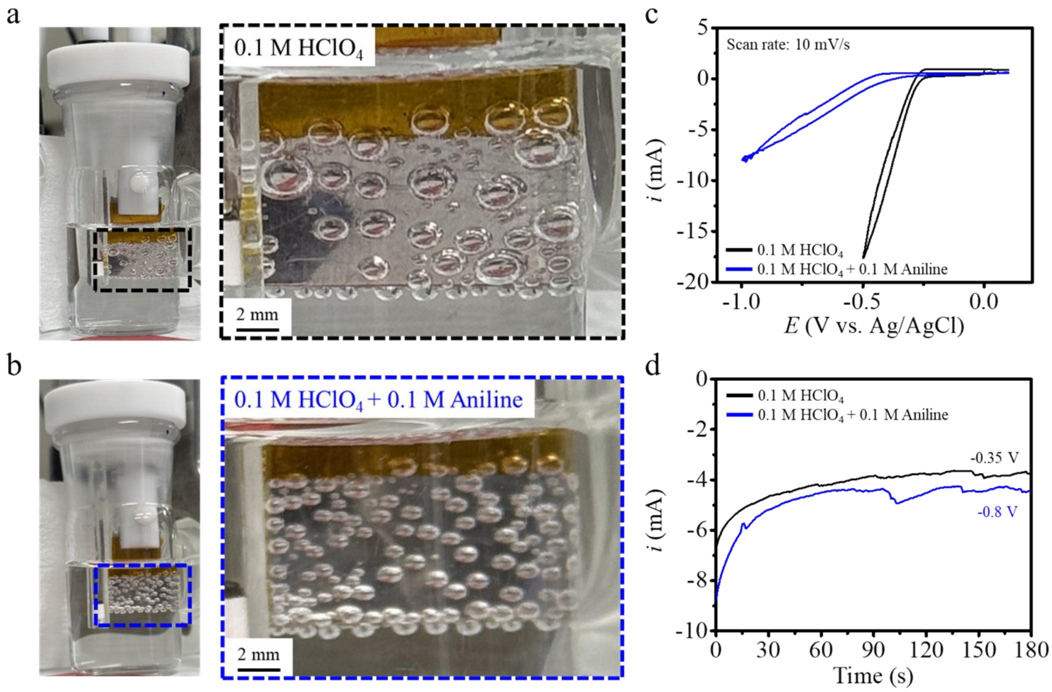

Figure S6. (a-b) Snapshots of hydrogen bubbles on Pt electrodes at ~180 s during the chronoamperometry in the two different solutions; hydrogen bubbles with smaller sizes were observed in the 0.1 M AnH$^+$ solution than in the 0.1 M HClO$_4$. (c) CVs of HER at 0.01 V/s measured in (black) 0.1 M HClO$_4$ and (blue) 0.1 M AnH$^+$, (d) chronoamperograms from each solution at the different E_{appl} to maintain nearly identical current density at quasi steady state.

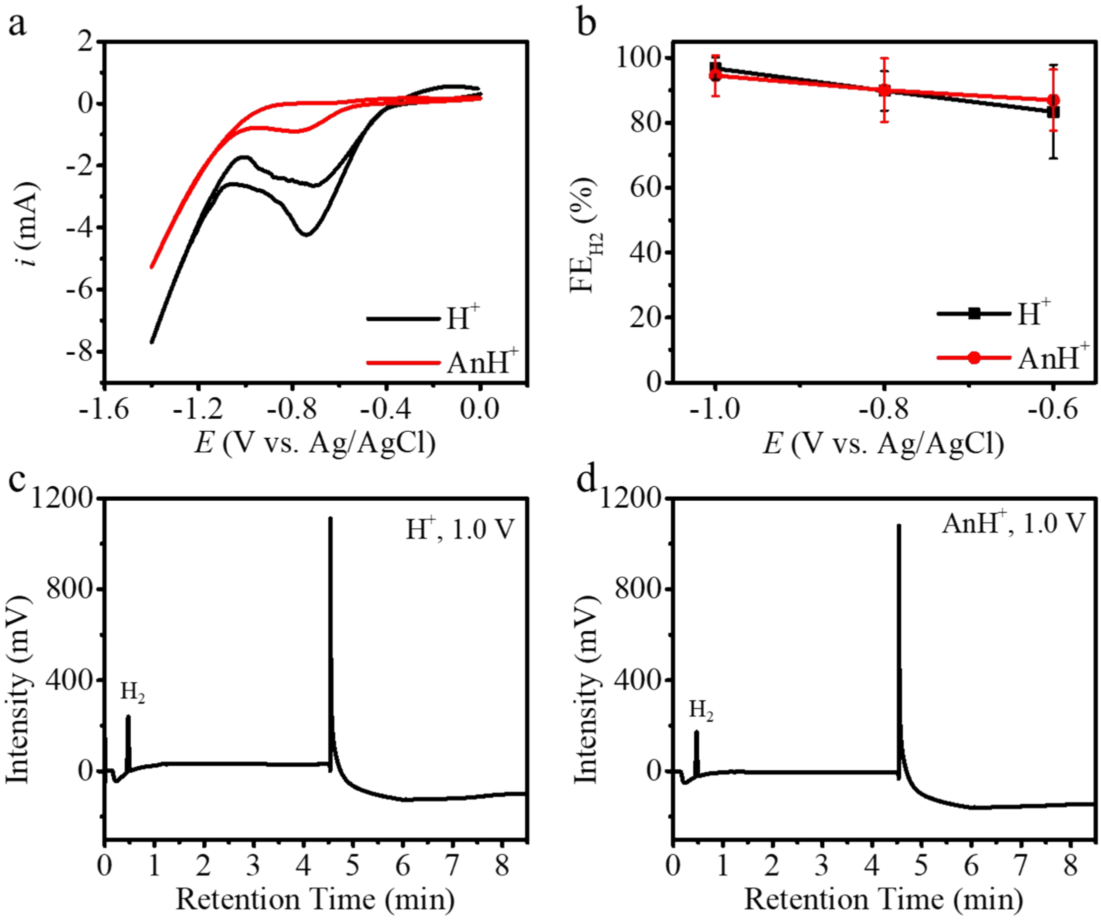

Figure S7. (a) CVs from the in situ GC electrochemical cell in solutions containing either 10 mM H^+ (black line) and the same concentration of AnH^+ (red line) at 20 mV/s, and (b) the resultant FE_{H2} vs. E_{appl} plots. GC spectra of obtained at –1.0 V vs. Ag/AgCl in (c) H^+ and (d) AnH^+ solutions.

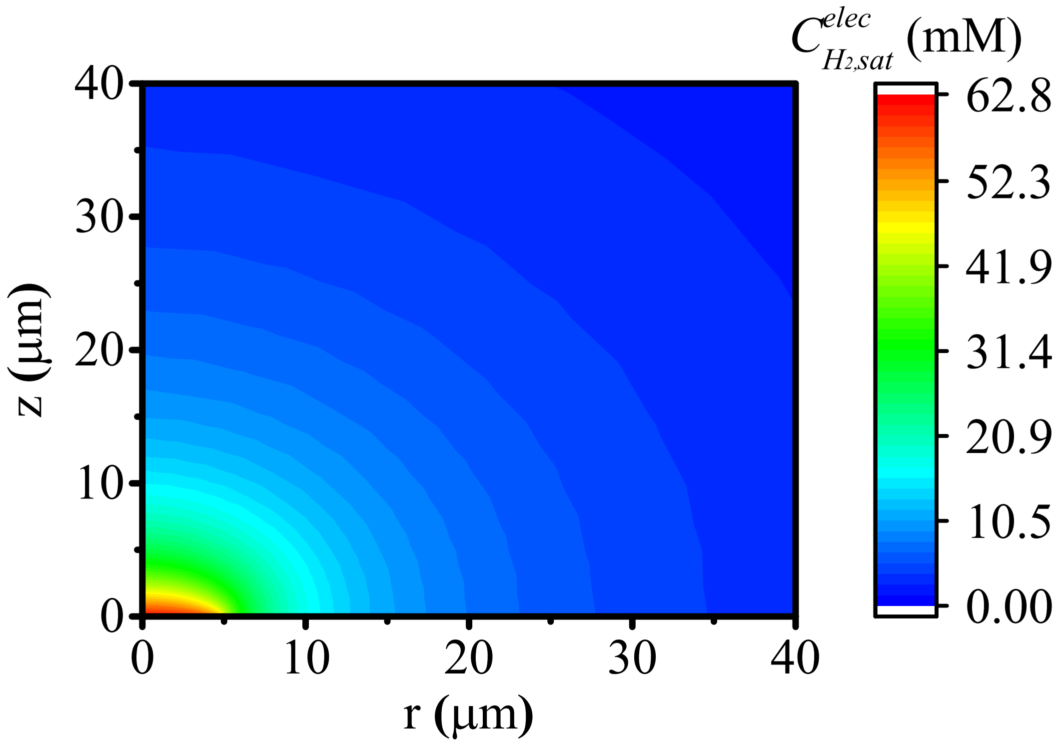

Figure S8. The simulated concentration profile at the maximum voltammetric current shown in Figure 3a.

Note S1. finite element method for voltammetric simulation for HER induced by H^+ and AnH^+-reduction on an UME

For voltammetric simulation through finite element method, a 2D axial domain was set to be square (500 x 500 μm^2) as schematically described in Figure S9. From the scheme, B1 represents the boundaries of the domain to maintain a constant $C_{\mathrm{H+}}$ or $C_{\mathrm{AnH+}}$ value. B2 represents an electrically insulating sheath. An electrode was depicted as a red line with its radius of 5 μm.

The flux of species was determined by Nernst-Planck equation with consideration of only diffusion in the domain. The electrode kinetics were determined by applying the Butler-Volmer kinetics. The scan rate of an electrode potential sweep set to be 20 mV/s. Reactions and the corresponding parameters for HER of H^+ and AnH^+ are listed in Table S4 and S5.

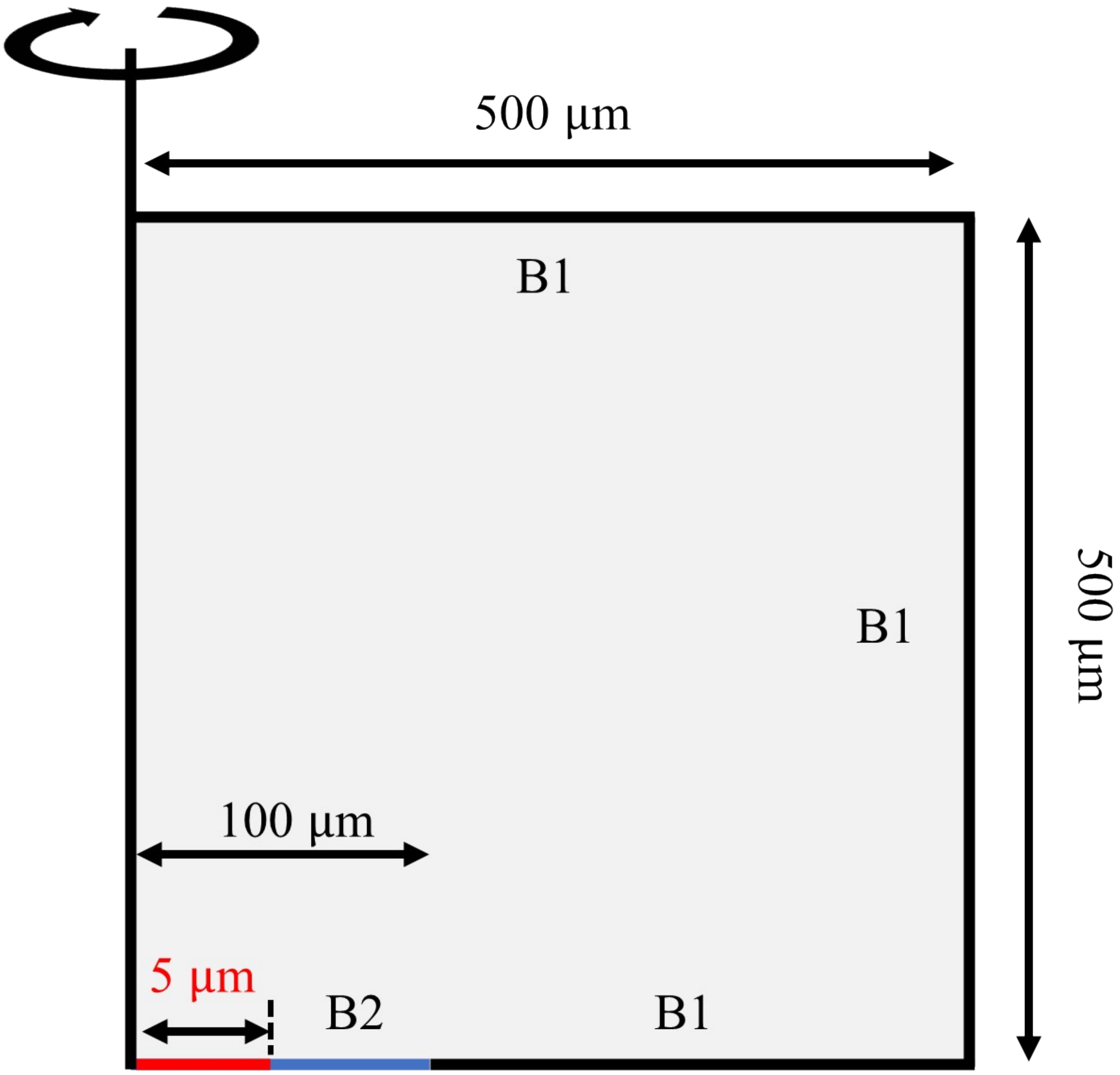

Figure S9. Description of the 2D axial domain of the finite element analysis for the voltammetric simulation.

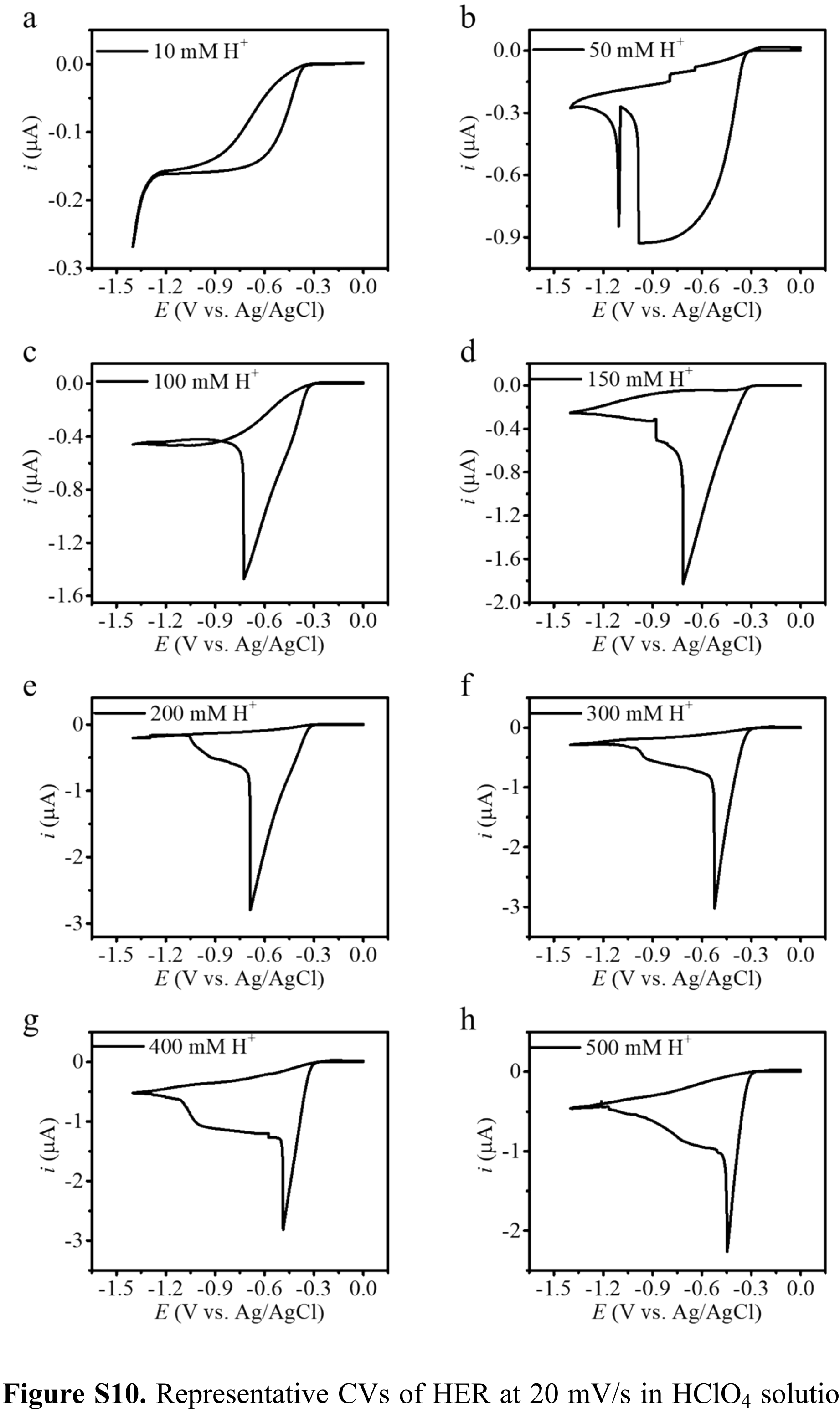

Figure S10. Representative CVs of HER at 20 mV/s in $HClO_4$ solutions with various $C_{H^+}^{bulk}$: (a) 10, (b) 50, (c) 100, (d) 150, (e) 200, (f) 300, (g) 400, and (h) 500 mM. We note that CVs at $C_{H^+}^{bulk}$ = 50 mM show the intermediate behavior, which gave either the limiting current or sudden current drop.

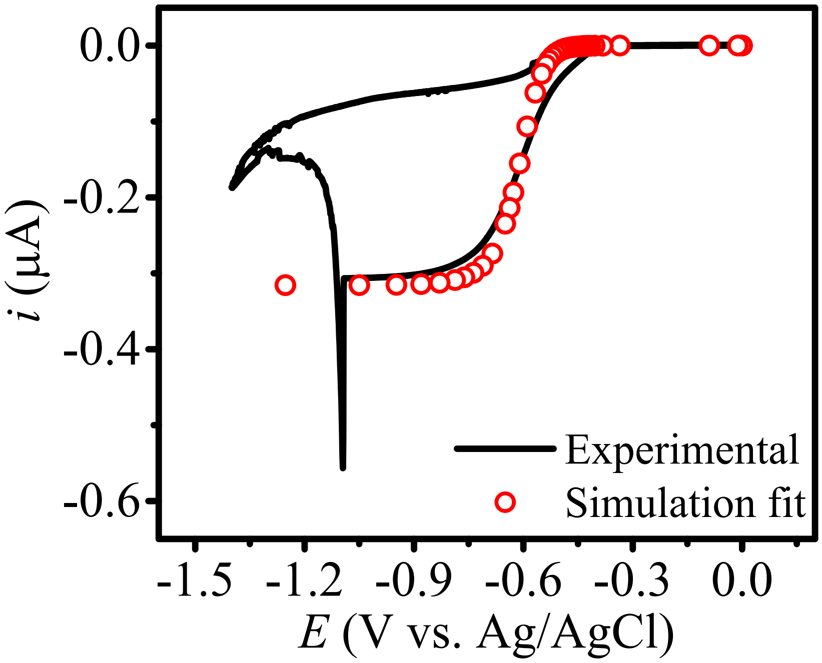

Figure S11. A CV at 20 mV/s in a 150 mM AnH^+ solution on a Pt UME and the voltammetric simulation result.

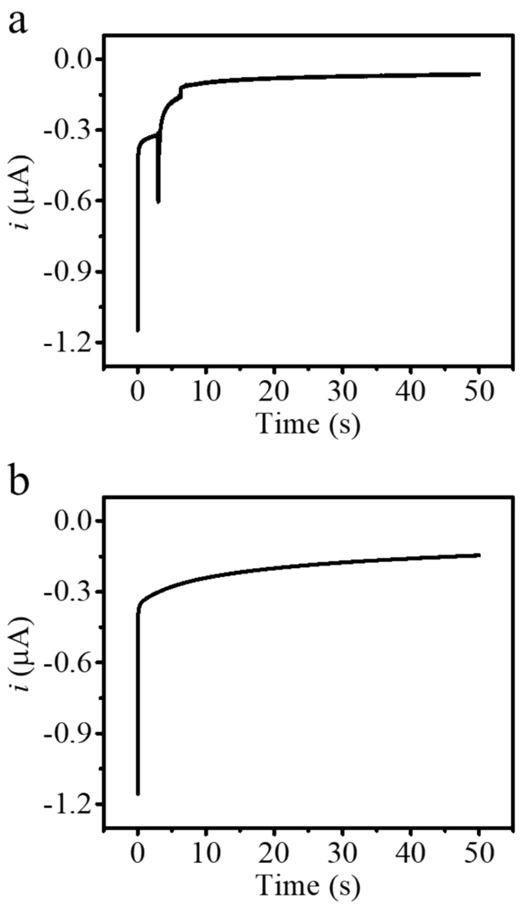

Figure S12. Representative *i-t* curves with/without the current spike measured from a same aqueous solution with 150 mM AnH^+ at E_{appl} = -0.95 V.

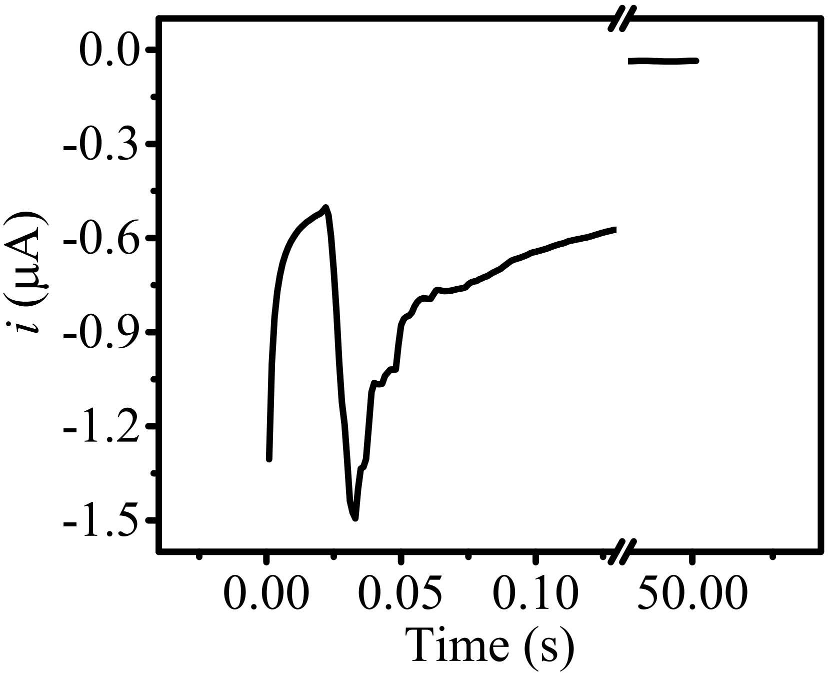

Figure S13. Representative *i*-*t* curve which was hard to resolve the t_{spike} of the current spike due to a capacitive current from aqueous solution with 150 mM AnH^+ at E_{appl} = -1.2 V.

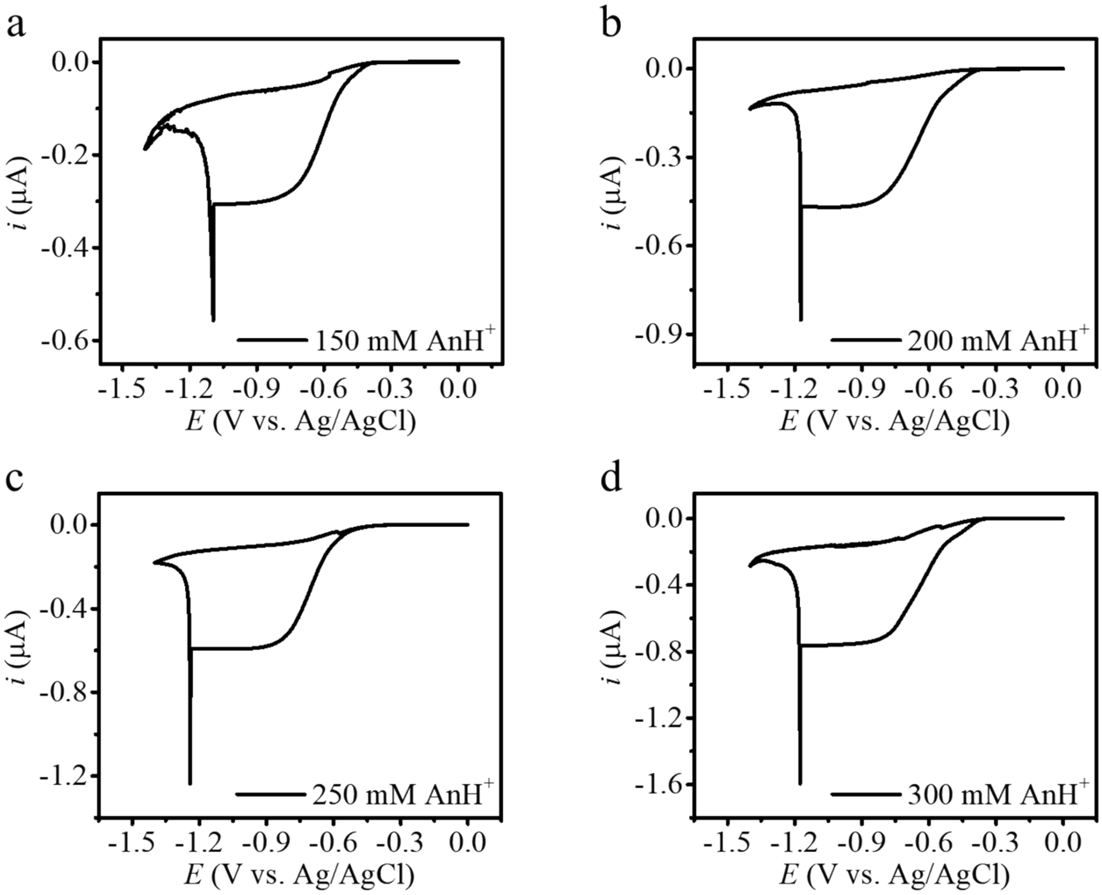

Figure S14. Representative CVs of HER at 20 mV/s in solutions with various concentration of AnH$^+$ = (a) 150, (b) 200, (c) 250, (d) 300 mM.

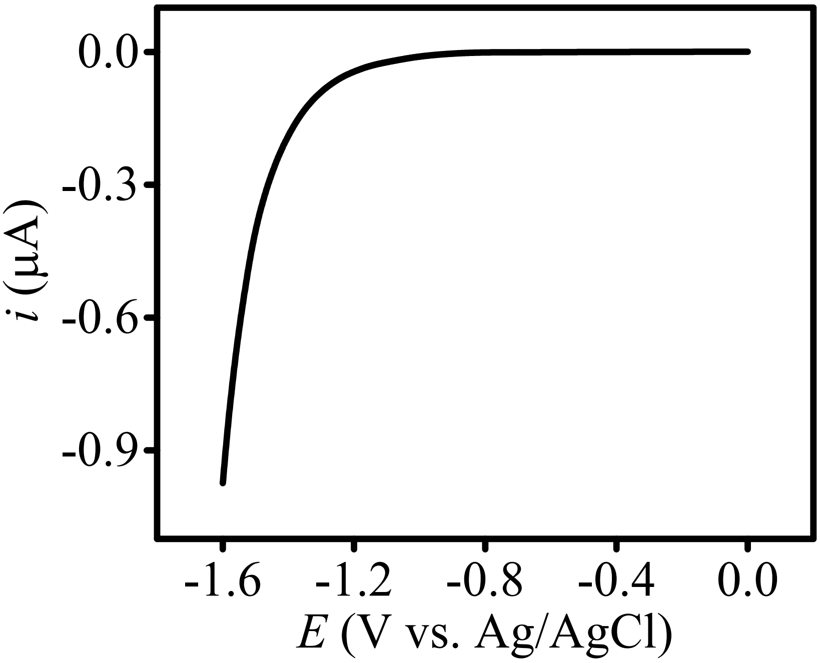

Figure S15. The background CV measured in 0.1 M $NaClO_4$ solution at 20 mV/s without either AnH^+ or An.

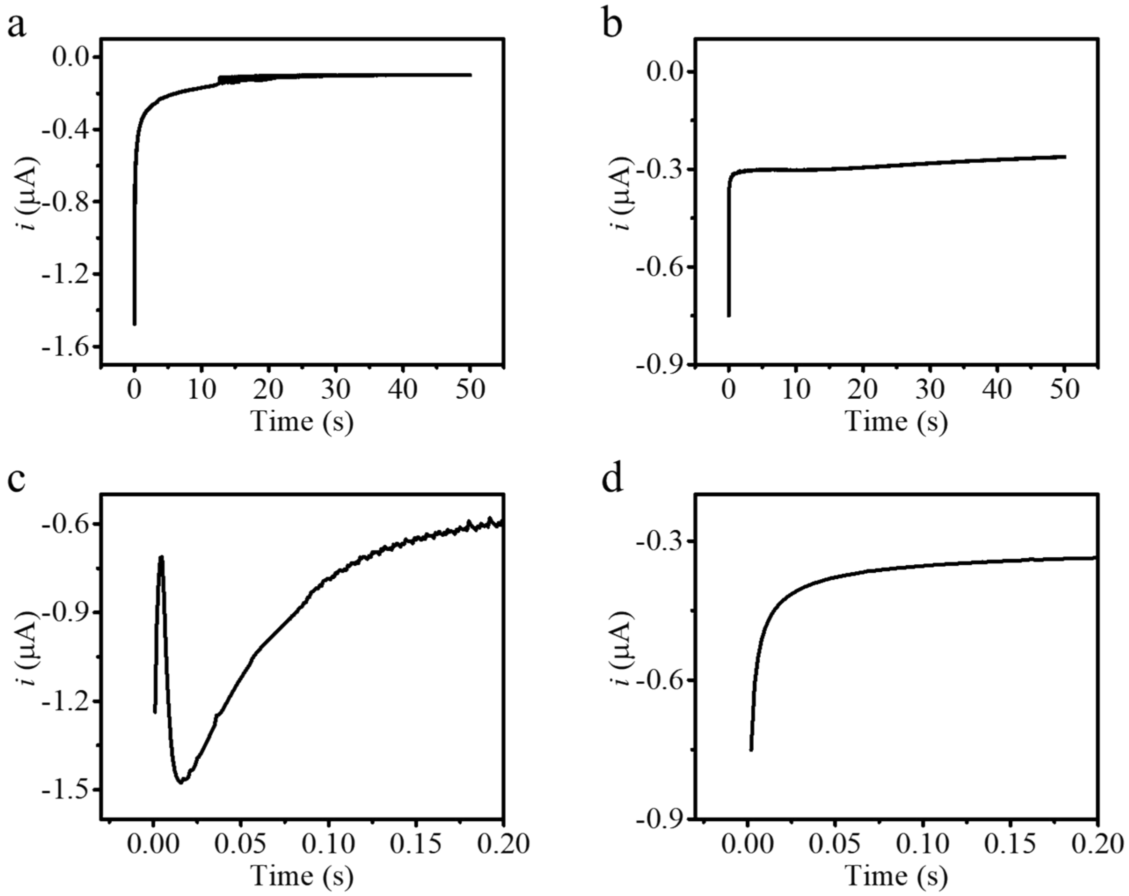

Figure S16. The representative *i-t* curves (a, c) with/(b, d) without a current spike asscociated with $[\mathrm{An\text{-}H}]_{\mathrm{ads}}$-reduction at $E_{\mathrm{appl}} = -1.3$ V in a 150 mM AnH^{+} solution with $C^{bulk}_{An}/C^{\ bulk}_{AnH^{+}} = 1$. (c) and (d) are the magnified *i-t* curves at $t \leq 0.2$ s from those in (a) and (b), respectively.

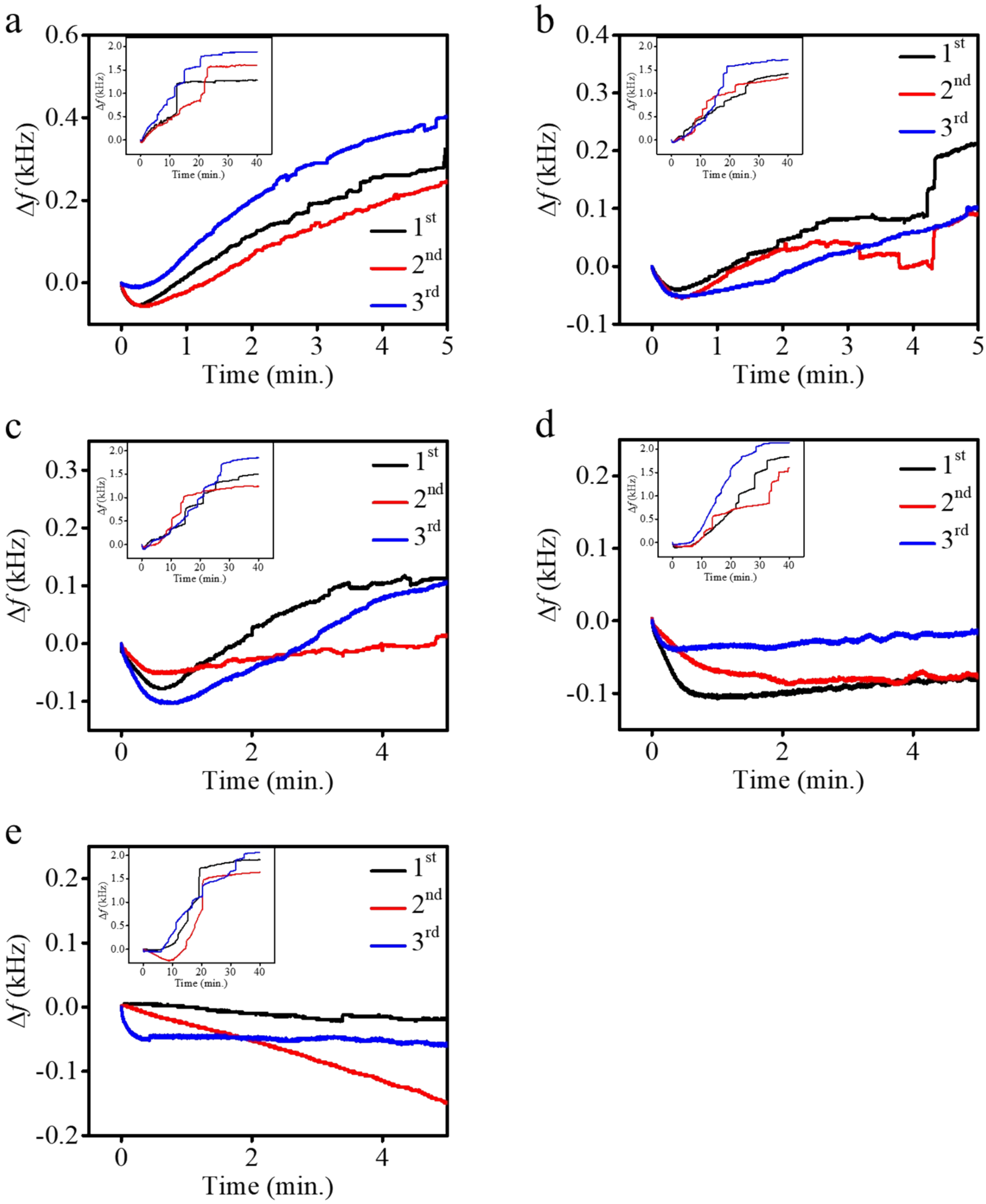

Figure S17. Δf vs. t curves with three replicates in solutions containing 50 mM AnH$^+$ with different C_{An}^{bulk} at E_{appl} = -0.8 V: C_{An}^{bulk} = (a) 0, (b) 25, (c) 50, (d) 100, and (e) 250 mM, respectively.

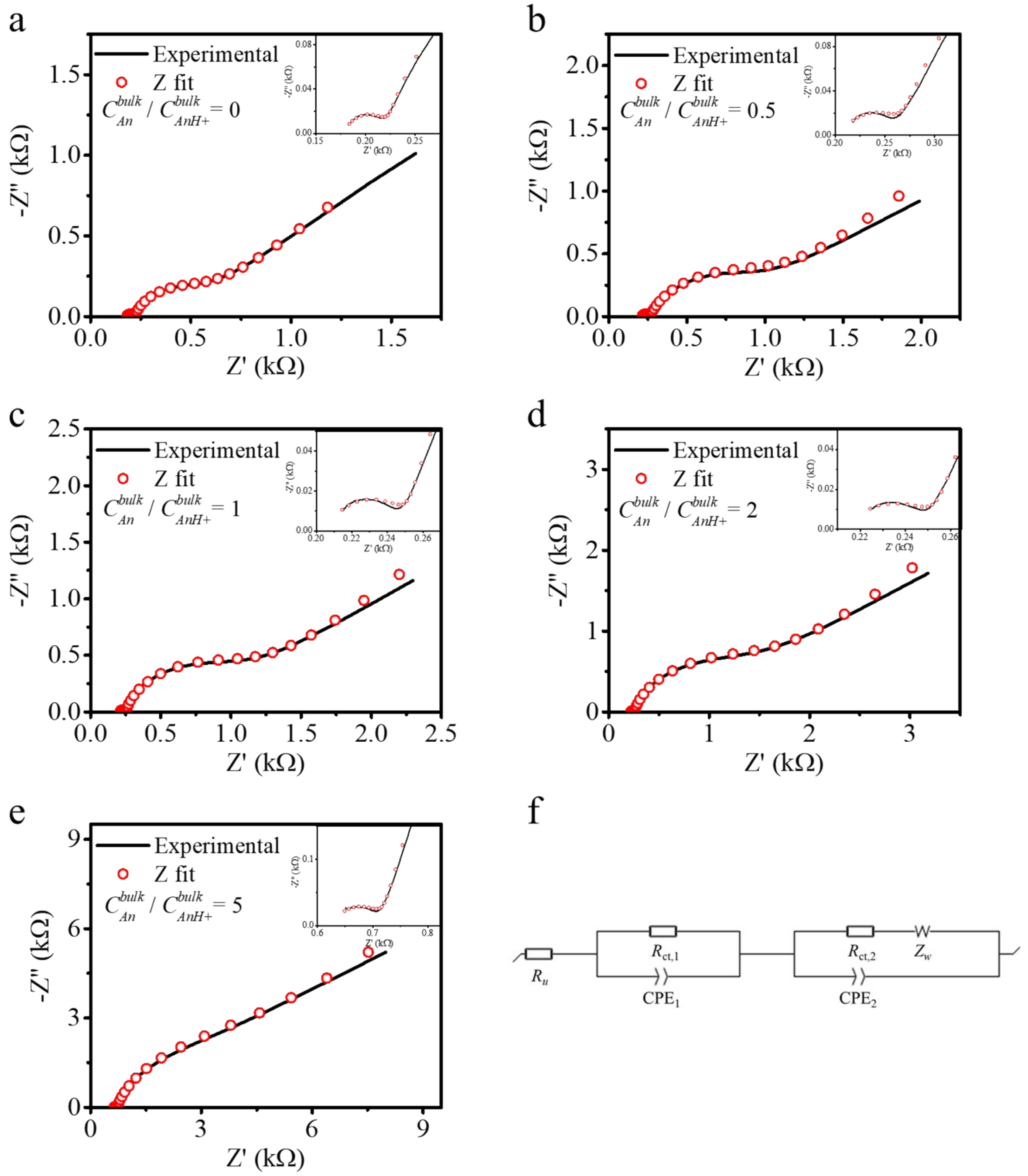

Figure S18. Representative Nyquist plots associated with HER of AnH$^+$ in different $C^{bulk}_{An}/C^{bulk}_{AnH^+}$ = (a) 0, (b) 0.5, (c) 1, (d) 2, and (e) 5 at $C^{bulk}_{AnH^+}$ = 50 mM, and (f) the equivalent circuit model for EIS simulation fitting to the experimental results. In this circuit model, $R_{ct,1}$ and $R_{ct,2}$ are the charge transfer resistance at an interface of Pt and that of $[An\text{-}H]_{ads}$, respectively. R_u is the uncompensated resistance, CPE is the constant phase element, and Z_w is the Warburg impedance.

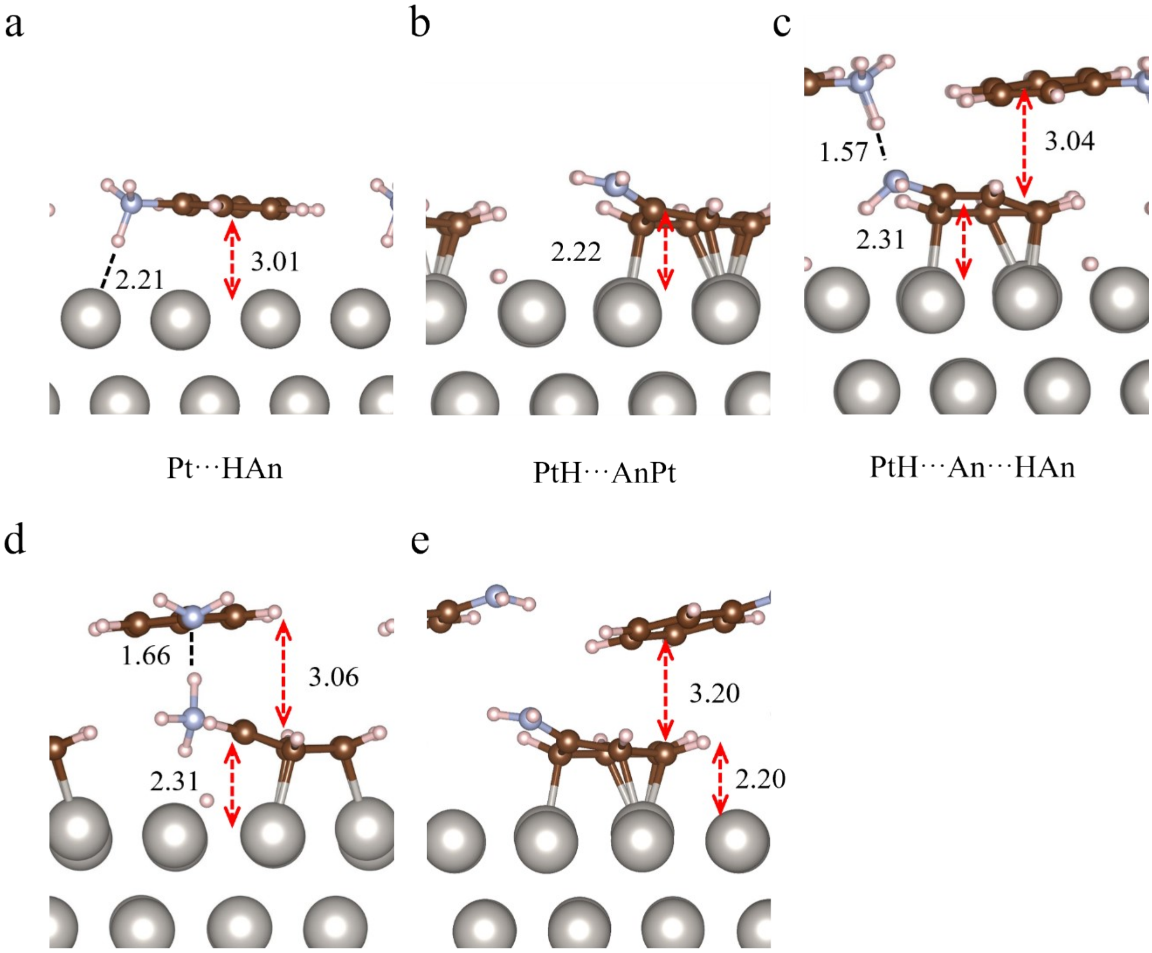

Pt···HAn

PtH···AnPt

PtH···An···HAn

PtH···AnH···An

PtAn···An

Figure S19. Enlarged figures of the corresponding geometries in the two-AnH adsorption mechanism. Hydrogen bonds are marked by black dashed lines, while height between the aromatic centers and Pt are marked by red arrow dashed lines.

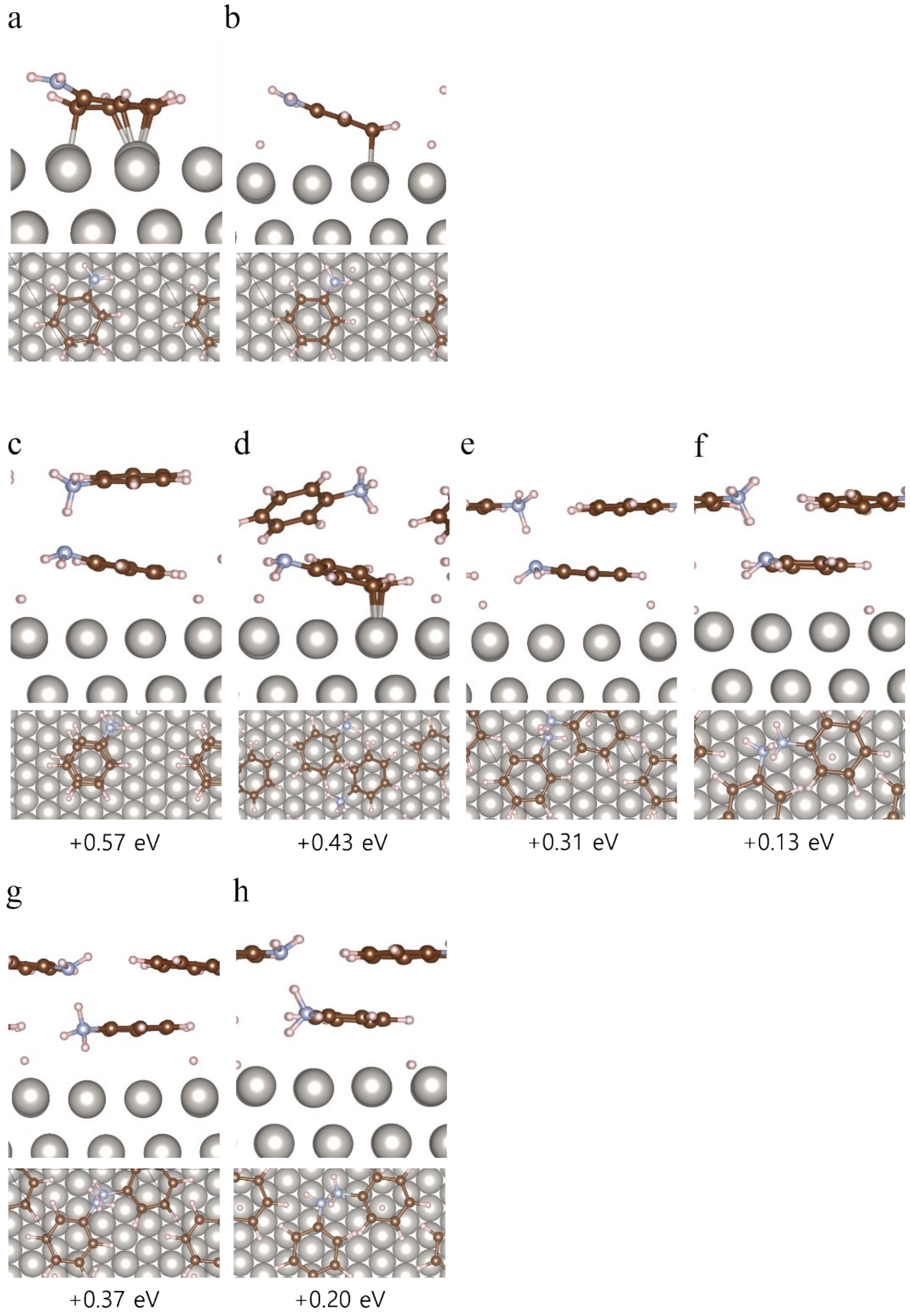

Figure S20. Alternative adsorption configurations evaluated using PBE-D3. (a) Adsorption of an An molecule. (b) Alternative adsorption configuration of PtH–An. (c–f) PtH–An–HAn structures optimized from different initial stacking directions, with H adsorbed on a Pt-top site (c–e) and a Pt-hollow site (f). (g, h) PtH–AnH–An structures with H adsorbed on a Pt-top site (g) and a Pt-hollow site (h). The numbers beneath each image indicate relative energies with respect to the most stable configurations shown in Fig. 6a.

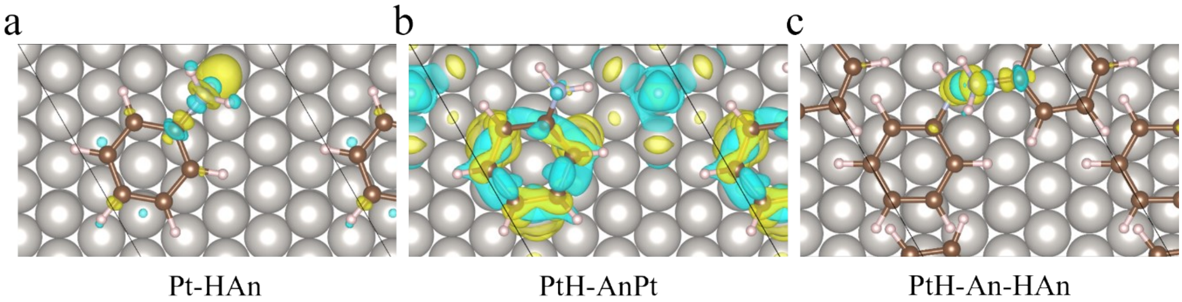

Pt-HAn PtH-AnPt PtH-An-HAn

Figure S21. Top view of the Charge density difference of adsorption of the three representative An(H), displaced in Figure 6c-e.

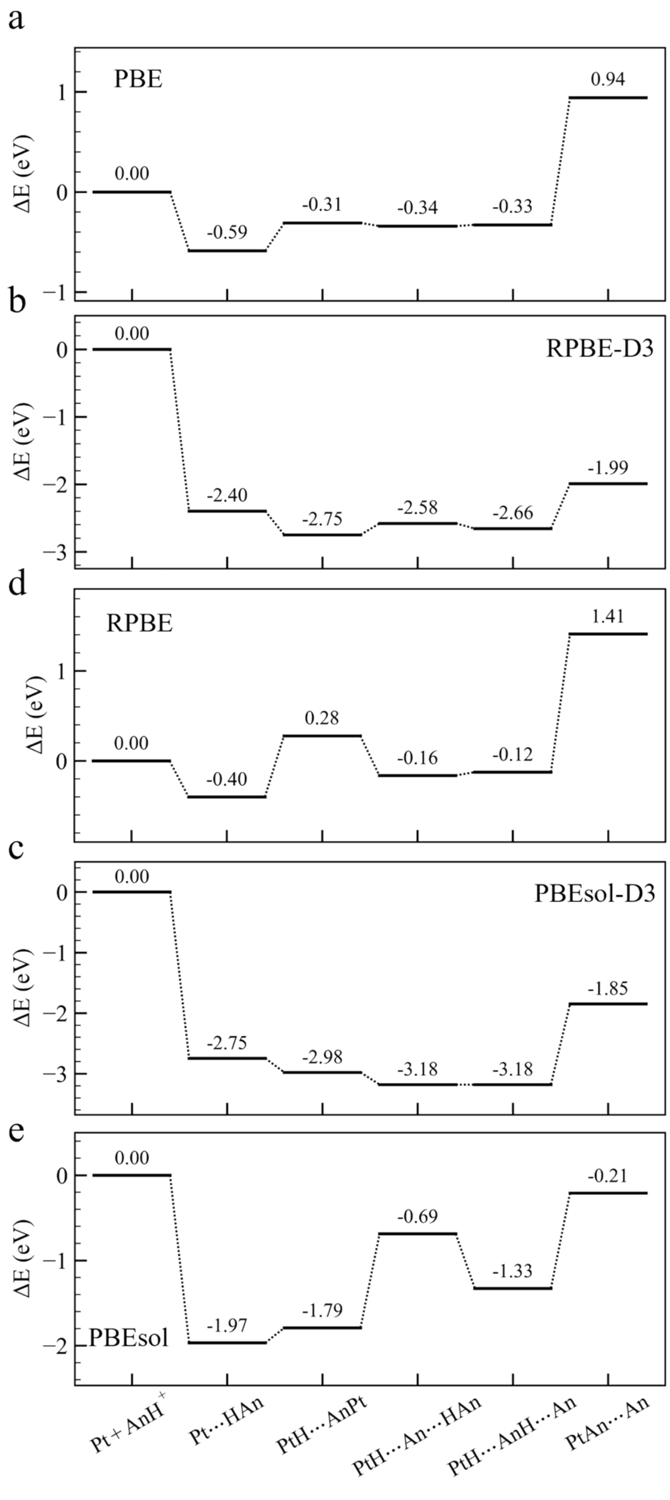

Figure S22 DFT calculated reaction diagrams for different functionals and application of dispersion corrections. (a) PBE, (b) RPBE. (c) RPBE-D3, (d) PBEsol, and (e) PBEsol-D3 at -0.56 V vs Ag/AgCl.

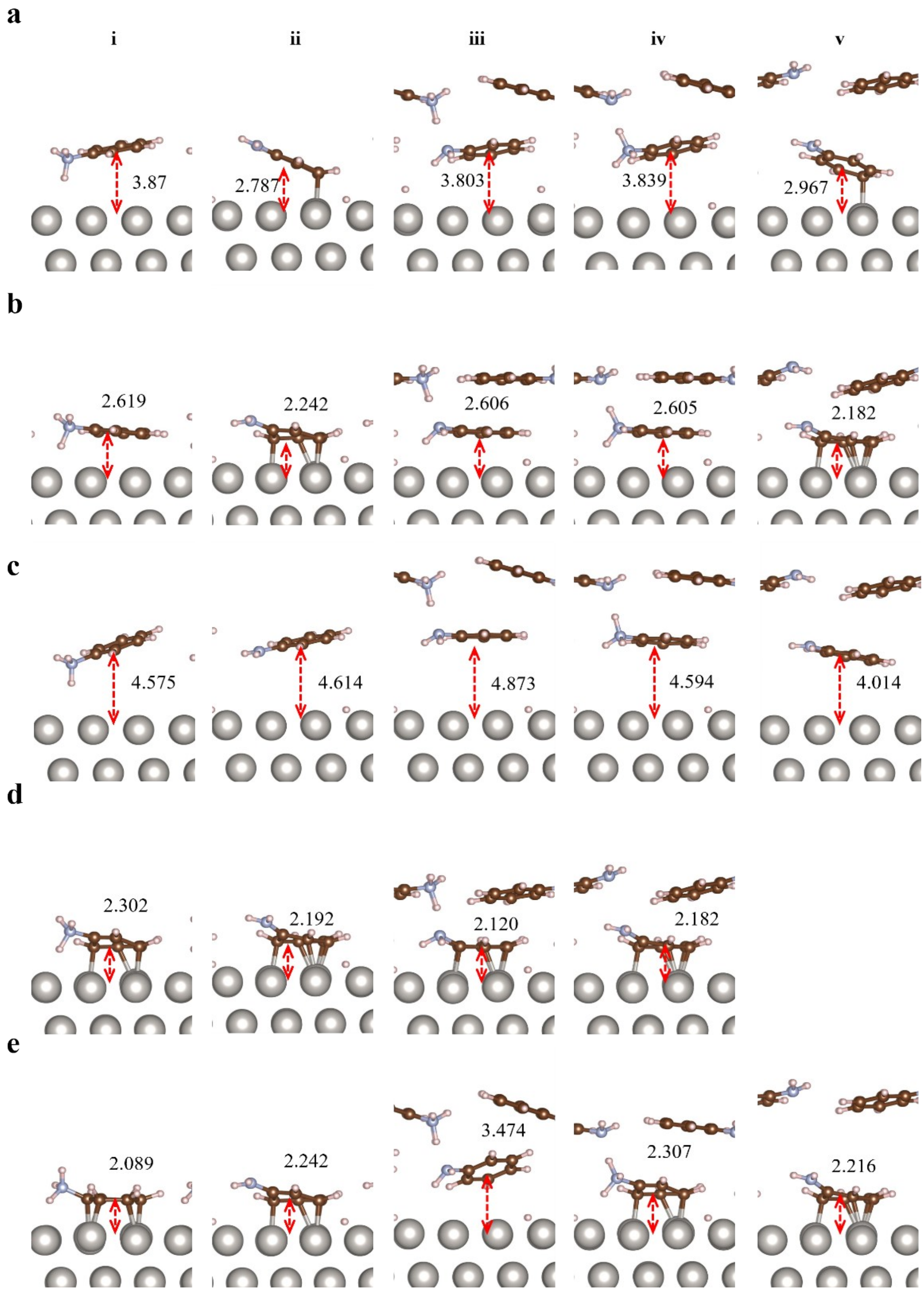

Figure S23 DFT optimized structures for different functionals and dispersion corrections. i-v indicates the reaction states corresponding to that of Figure 6a. Each row corresponds to (a) PBE, (b) RPBE-D3, (c) RPBE, (d) PBEsol-D3, and (e) PBEsol, where i-v correspond to the structures found in Figure 6. Note for e, only four structures are shown, omitting PtH···AnH···An (the iv structure), which after optimization falls back to PtH···An···HAn (iii). The heights between the aromatic centers and Pt are marked by red arrow dashed lines with corresponding distances (Å).

Note S2. Comparison of different functionals and dispersion corrections

To assess the validity of our DFT calculations, we employed the PBE, RPBE, and PBEsol functionals with Grimme's D3(BJ) dispersion corrections.[1, 2] These combinations have been widely tested on surface–molecule interfaces and offer faster performance than non-local vdW functionals. Geometry optimizations were performed based on the most stable structures identified from PBE-D3(BJ) calculations along the reaction pathway shown in Figure 6a (see Figures S22–S23).

The corresponding lattice constants for FCC Pt structures, obtained using Birch–Murnaghan fitting, were 3.968 Å (PBE), 3.916 Å (RPBE), 3.880 Å (RPBE-D3), 3.990 Å (PBEsol), and 3.780 Å (PBEsol-D3). Figure S22 compares the relative energies of the adsorbed configurations. A reference potential of –4.6 V vs. SHE was applied across all functionals. Without dispersion corrections, the optimized structures exhibited large intermolecular distances (Table S6), indicating weak physisorption (Figure S23).

In particular, the PBE and RPBE geometries (Figure S23a, b) suggest that the AnH–Pt interaction is primarily through the ammonium group. When dispersion corrections are included, the benzene ring becomes the main adsorption site, reflected by lower adsorption energies and shorter Pt–An1 distances.

Figure S22 also shows that without dispersion, the enthalpy change for adsorption from state i to ii (Pt···HAn → PtH···AnPt) is positive: 0.27 eV (PBE), 0.68 eV (RPBE), and 0.22 eV (PBEsol). However, with D3 corrections, the values shift to -0.42, –0.35, and –0.23 eV, respectively. This substantial change underscores the necessity of including dispersion effects when modeling reduced AnH species at the surface.

Additionally, across all functionals, the second AnH reduction step was thermodynamically unfavorable at the applied potential without dispersion, but generally became more favorable upon including D3 corrections. This indicates that multilayer adsorption structures are stabilized primarily by dispersion interactions.

Notably, dispersion corrections also introduced substantial structural differences. For instance, the Pt–An height varied by ~1 Å in PBE and ~2 Å in RPBE, while PBEsol showed minimal change. These trends reflect the nature of each functional: RPBE was developed to mitigate PBE's overbinding, while PBEsol tends to overbind molecule–surface systems, potentially making it unsuitable for accurately describing adsorption.[3] This is evident in the PBEsol geometries (Figure S23e), where the benzene ring strongly adheres to the Pt surface, forming bent structures indicative of σ-type partial hybridization even in the absence of dispersion corrections.

Direct experimental benchmarks for An/AnH adsorption enthalpies or high-level quantum cluster calculations remain technically challenging, complicating absolute validation of functional performance. Nonetheless, our systematic comparison across PBE, RPBE, and

PBEsol, with and without D3 corrections, establishes a consistent internal scale for evaluating dispersion contributions. These findings emphasize the need for incorporating dispersion to accurately model electrochemically reduced, protonated organic layers. Further semi-quantitative validation methods, such as ITC titrations or many-body DFT calculations, would aid in refining absolute adsorption energetics.

Table S1. The simulation parameters for electrode reaction and chemical reaction in Figure 1c; the standard reduction potential, transfer coefficient, standard electron transfer rate constant, equilibrium constant, forward rate constant, diffusion coefficients and concentrations of species, *i* are designated as E^{o}, α, k^{0}, K_{eq}, k_{f}, D_{i}, and C_{i}, respectively.

Reactions	Parameters
$H^{+} + e^{-} \rightleftharpoons H\cdot$	$E^{0} = -0.46$ V, $\alpha = 0.5$, $k^{0} = 0.1$ cm/s
$H\cdot + H\cdot \rightleftharpoons H_{2}$	$K_{eq} = 10^{4}$, $k_{f} = 10^{7}$
Diffusion coefficients and initial concentrations of all species	
$D_{H+} = D_{H\cdot} = D_{H2} = 9.3 \times 10^{-5}$ cm^{2}/s, $C_{H+} = 10$ mM, $C_{H\cdot} = C_{H2} = 0$ mM.	

Table S2. The simulation parameters for electrode reaction and chemical reaction through CE process in Figure 1c.

<table>
<tr><th>Reactions</th><th>Parameters</th></tr>
<tr><td>$H^+ + e^- \rightleftharpoons H\cdot$</td><td>$E^0 = -0.46$ V, $\alpha = 0.5$, $k^0 = 0.1$ cm/s</td></tr>
<tr><td>$AnH^+ \rightleftharpoons An + H^+$</td><td>$K_{eq} = 10^{-4.63}$, $k_f = 5 \times 10^2$</td></tr>
<tr><td>$H\cdot + H\cdot \rightleftharpoons H_2$</td><td>$K_{eq} = 10^4$, $k_f = 10^7$</td></tr>
<tr><td colspan="2">Diffusion coefficients and initial concentrations of all species</td></tr>
<tr><td colspan="2">$D_{H+} = D_{H\cdot} = D_{H2} = 9.3 \times 10^{-5}$ cm^2/s, $D_{AnH+} = D_{AnH\cdot} = D_{An} = 1.1 \times 10^{-5}$ cm^2/s
$C_{H+} = 10$ mM, $C_{H\cdot} = C_{H2} = 0$ mM.</td></tr>
</table>

Table S3. The simulation parameters for electrode reaction and chemical reaction through combined CE + EC process in Figure 1c.

Reactions	**Parameters**
$H^+ + e^- \rightleftharpoons H\cdot$ $AnH^+ + e^- \rightleftharpoons AnH\cdot$	$E^0 = -0.46$ V, $\alpha = 0.5$, $k^0 = 0.1$ cm/s $E^0 = -0.73$ V, $\alpha = 0.5$, $k^0 = 0.1$ cm/s
$AnH^+ \rightleftharpoons An + H^+$ $H\cdot + H\cdot \rightleftharpoons H_2$	$K_{eq} = 10^{-4.63}$, $k_f = 5 \times 10^2$ $K_{eq} = 10^4$, $k_f = 10^7$
Diffusion coefficients and initial concentrations of all species	
$D_{H+} = D_{H\cdot} = D_{H2} = 9.3 \times 10^{-5}\ cm^2/s$, $D_{AnH+} = D_{AnH\cdot} = D_{An} = 1.1 \times 10^{-5}\ cm^2/s$ $C_{H+} = 10$ mM, $C_{H\cdot} = C_{H2} = 0$ mM.	

Table S4. The simulation parameters for electrode reaction and chemical reaction in Figure 3.

Reactions	**Parameters**
$H^+ + e^- \rightleftharpoons H\cdot$	$E^0 = -0.46$ V, $\alpha = 0.5$, $k^0 = 0.1$ cm/s
$H\cdot + H\cdot \rightleftharpoons H_2$	$K_{eq} = 10^4$, $k_f = 10^7$
Diffusion coefficients and initial concentrations of all species	
$D_{H+} = D_{H\cdot} = D_{H2} = 9.3 \times 10^{-5}$ cm^2/s, $C_{H+} = 150$ mM, $C_{H\cdot} = C_{H2} = 0$ mM.	

Table S5. The simulation parameters for electrode reaction and chemical reaction in Figure S11.

Reactions	Parameters
$\mathrm{AnH^+ + e^- \rightleftharpoons AnH\cdot}$	$E^0 = -0.6$ V, $\alpha = 0.5$, $k^0 = 0.1$ cm/s
$\mathrm{2AnH\cdot \rightleftharpoons 2An + H_2}$	$K_{eq} = 10^4$, $k_f = 10^7$
Diffusion coefficients and initial concentrations of all species	
$D_{\mathrm{AnH+}} = D_{\mathrm{AnH\cdot}} = D_{\mathrm{An}} = 1.1 \times 10^{-5}$ cm^2/s $C_{\mathrm{AnH+}} = 150$ mM, $C_{\mathrm{AnH\cdot}} = C_{\mathrm{An}} = C_{\mathrm{H2}} = 0$ mM.	

Table S6. Optimized structural parameters for the various An and AnH configurations in different functionals, represented in Figure 6a and Figure S23.

XC	Moiety	h(Pt-An1) [Å]	h(An-An) [Å]	h(Pt-N1) [Å]	h(Pt-N2) [Å]	d(Pt-H1) [Å]	d(N1-H1) [Å]	d(N1-H2) [Å]	d(N2-H2) [Å]
PBE-D3	Pt···HAn	3.010	-	3.100	-	2.211	1.079	-	-
	PtH···AnPt	2.224	-	3.118	-	1.854	4.049	-	-
	PtH···An···HAn	2.313	3.040	2.968	5.481	1.848	3.557	1.568	1.124
	PtH···AnH···An	2.313	3.063	2.921	5.462	1.840	3.566	1.092	1.660
	*An-An	2.195	3.200	3.015	6.133	-	-	-	-
PBE	Pt···HAn	3.870	-	3.343	-	2.496	1.057	-	-
	PtH···AnPt	2.787	-	3.772	-	1.865	4.025	-	-
	PtH···An···HAn	3.801	3.242	3.762	6.424	1.868	4.447	1.703	1.094
	PtH···AnH···An	3.839	3.229	3.727	6.369	1.867	4.491	1.093	1.711
	*An-An	2.967	4.413	3.998	7.905	-	-	-	-
RPBE-D3	Pt···HAn	2.619	-	2.900	-	2.039	1.102	-	-
	PtH···AnPt	2.242	-	3.016	-	1.870	3.188	-	-
	PtH···An···HAn	2.606	2.783	2.852	5.395	1.867	3.482	1.624	1.108
	PtH···AnH···An	2.605	2.831	2.837	5.366	1.851	3.475	1.086	1.690
	*An-An	2.163	3.010	2.895	6.012	-	-	-	-
RPBE	Pt···HAn	4.575	-	3.569	-	2.839	1.044	-	-
	PtH···AnPt	4.614	-	4.022	-	1.556	2.996	-	-
	PtH···An···HAn	4.873	3.510	4.961	7.706	1.557	3.676	1.758	1.082
	PtH···AnH···An	4.594	3.401	4.856	7.611	1.557	3.624	1.081	1.761
	*An-An	4.014	3.691	4.518	8.359	-	-	-	-
PBEsol-D3	Pt···HAn	2.302	-	2.947	-	2.135	1.100	-	-
	PtH···AnPt	2.192	-	3.140	-	1.852	4.060	-	-
	PtH···An···HAn	2.120	2.802	2.702	5.273	1.860	3.429	1.510	1.148
	PtH···AnH···An	-	-	-	-	-	-	-	-
	*An-An	2.182	2.955	2.987	5.884	-	-	-	-
PBEsol	Pt···HAn	2.089	-	2.729	-	2.166	1.073	-	-
	PtH···AnPt	2.242	-	3.016	-	1.870	3.188	-	-
	PtH···An···HAn	3.474	3.377	3.458	6.084	1.848	4.214	1.649	1.110
	PtH···AnH···An	2.307	3.499	2.990	5.484	1.834	3.529	1.106	1.644
	*An-An	2.216	5.112	3.170	7.856	-	-	-	-

Each row corresponds to one adsorbed system, labeled by an internal code (e.g., “Pt···HAn ”). h(X–Y) denotes the perpendicular (vertical) distance, in Å, from X to Y, typically measured relative to the Pt plane or ring centroid. d(X–Y) denotes the direct interatomic or bond distance, in Å, between X and Y. Subscripts (e.g., N1, N2, H1, H2) refer to specific atoms in the molecule being the nitrogen in the first and second Aniline, and hydrogens originating from the first and second cationic aniline, respectively.

References

1. B. Hammer, L. B. Hansen and J. K. Nørskov, *Phys. Rev. B*, 1999, **59**, 7413-7421.
2. J. P. Perdew, A. Ruzsinszky, G. I. Csonka, O. A. Vydrov, G. E. Scuseria, L. A. Constantin, X. Zhou and K. Burke, *Phys. Rev. Lett.*, 2008, **100**, 136406.
3. A. Stroppa and G. Kresse, *New J. Phys.*, 2008, **10**, 063020.